IEEE Access
Multidisciplinary | Rapid Review | Open Access Journal

Received November 27, 2020, accepted December 18, 2020, date of publication December 29, 2020,
date of current version January 15, 2021.

*Digital Object Identifier 10.1109/ACCESS.2020.3047951*

# Surface Temperature Retrieval From Gaofen-5 Observation and Its Validation

**ENYU ZHAO[1], QIJIN HAN[2], AND CAIXIA GAO[3]**

[1]College of Information Science and Technology, Dalian Maritime University, Dalian 116026, China
[2]China Centre for Resources Satellite Data and Application, Beijing 100094, China
[3]Key Laboratory of Quantitative Remote Sensing Information Technology, Aerospace Information Research Institute, Chinese Academy of Sciences, Beijing 100094, China

Corresponding author: Caixia Gao (gaocaixia@aoe.ac.cn)

This work was supported in part by the National Natural Science Foundation of China under Grant 41801231 and Grant 41671370, and in part by the Fundamental Research Funds for the Central Universities under Grant 3132019341.

**ABSTRACT** Surface temperature (ST) plays a great role in urban heat island effect, environment monitoring, earth resources monitoring, and water balance at local and global scales. The Chinese Gaofen-5 (GF5) satellite can capture Earth's thermal infrared information for use in national high-resolution Earth observations. In this article, the nonlinear split-window algorithm and the refined generalized split-window method are used to retrieve sea surface temperature (SST) and land surface temperature (LST) from GF5 observations. For different atmospheric and surface conditions, the algorithm coefficients are calculated using a statistical regression method from the numerical values simulated with the atmospheric radiative transfer model MODTRAN 5.0. The simulation results show that the root mean square error (RMSE) for SST and LST retrieval ranges from 0.09 K to 0.46 K and 0.19 K to 0.69 K, respectively, with increasing water vapor content (WVC). To validate the retrieved STs, Moderate Resolution Imaging Spectroradiometer (MODIS) STs extracted from the MYD11A1 product are used. Note that the RMSEs of both the LST and SST are less than 3.3 K. The RMSE for SST retrieval varies from 1.2 K to 1.45 K, with a mean value of 1.33 K; the RMSE for LST retrieval ranges from 1.57 K to 3.3 K, with a mean value of 2.41 K.

**INDEX TERMS** Surface temperature, Gaofen-5, thermal infrared.

## I. INTRODUCTION

Surface temperature (ST), which includes land surface temperature (LST) and sea surface temperature (SST), is a significant parameter for monitoring the changes in earth resources and one of the most critical indicators in the physical process of surface energy at local and global scales [1]–[6]. The ST can provide information on the spatiotemporal changes of the state of the surface [7]–[11]. It has been widely used in research fields such as numerical prediction, global circulation models, regional and global climate studies, geology, oceanography and vegetation monitoring [12]–[17]. Accurate ST contributes to assessing the surface energy, hydrological balance, and soil moisture [10], [18]–[23]. Fortunately, since the development of remote sensing in the last three decades, some infrared sensors including Gaofen-5 (GF5), Visible Infrared Imaging Radiometer Suite (VIIRS), Moderate Resolution Imaging Spectroradiometer (MODIS), etc., have provided us with a reliable data source to obtain ST over the entire globe.

To date, a large number of methods have been proposed to retrieve LST and SST from thermal infrared (TIR) remotely sensed data. McMillin first proposed a split-window (SW) algorithm to retrieve SST from two satellite TIR channels without atmospheric profile information [24]. Subsequently, many algorithms were developed to successfully obtain SST. Additionally, with the development of remote sensing applications, scientists have proposed many methods to retrieve LST based on the approximation and hypothesis of the atmospheric radiation transfer model. Some scientists extended the SW algorithm to LST retrieval with the knowledge of land surface emissivity (LSE), such as the linear SW algorithm and nonlinear SW algorithm. Wan *et al.* proposed a generalized split-window (GSW) method that is widely used to retrieve LST based on the differential water vapor absorption in two adjacent TIR channels [25].

The Chinese GF5 satellite with Multiple Spectral-Imager (MSI) payload, which was launched on May 9, 2018, is the

The associate editor coordinating the review of this manuscript and approving it for publication was Stefania Bonafoni.

fifth satellite of the China High-resolution Earth Observation System (CHEOS). The orbit altitude is 705 km, and the local time of the ascending node is 13:30. The satellite has four TIR channels centered at 8.20 $\mu$m (channel 9: 8.01–8.39 $\mu$m), 8.63 $\mu$m (channel 10: 8.42–8.83 $\mu$m), 10.80 $\mu$m (channel 11: 10.30–11.30 $\mu$m), and 11.95 $\mu$m (channel 12: 11.40–12.50 $\mu$m), with a 40 m spatial resolution. There are two terrestrial observation payloads and four atmospheric observation payloads on the GF5 satellite, which enable the GF5 satellite to be used for air pollution, inland water bodies, terrestrial surface ecological environment, mineral exploration and other aspects [26]–[30], [32], [32].

Over the past two years, some methods have been proposed to retrieve LST or SST from simulated GF5 data. For example, Chen *et al.* used the semiempirical quadratic SW equation to retrieve SST from simulated GF5 data, and a bias of −0.05 K and a root mean square error (RMSE) of 0.53 K were obtained [28]. Tang developed nonlinear SW algorithms to estimate LST and SST from simulated Chinese GF5 satellite data, and the results showed that the methods are appropriate, with an RMSE of 0.7 K for LST retrieval and an RMSE of 0.3 K for SST retrieval [33]. Ye *et al.* proposed a four-channel method to retrieve LST from GF5 data simulated from Thermal Airborne Spectrographic Imager (TASI) data with an RMSE less than 1 K [34]. Ren *et al.* used a hybrid algorithm to retrieve LST and LSE with simulated GF5 data, and the results showed that this method can obtain an RMSE less than 1 K and 0.015, respectively [35]. Meng *et al.* used the real GF5 data to obtain LST and SST, the retrieval results were relatively ideal cross-validated by Moderate-resolution Imaging Spectroradiometer (MODIS) LST/SST, Visible infrared Imaging Radiometer (VIIRS) LST/SST, and Advanced Himawari Imager (AHI) SST products [26]. However, LST and SST retrieved from the simulated data can obtain acceptable results, but these retrieval methods used on the real GF5 data still need to be further verified with sufficient images. The objective of this article is to evaluate the LST and SST retrieval approaches applied to real GF5 TIR observations based on different test sites.

This article is organized as follows: Section 2 describes the methodology for the LST and SST retrieval methods. In Section 3, the retrieval algorithms are applied GF5 data, and the results are validated with MODIS LST products. The conclusions are presented in Section 4.

## II. METHODOLOGY AND SIMULATION DATASETS

### A. THERMAL RADIATIVE TRANSFER EQUATION

From the radiative transfer theory, for a cloud-free atmosphere under local thermodynamic equilibrium, the radiative transfer equation (RTE) in the TIR channel can be written as [36]

$$B_i(T_i) = \tau_i \left[ \varepsilon_i B_i(T_s) + (1 - \varepsilon_i) R^{\downarrow}_{atm\_i} \right] + R^{\uparrow}_{atm\_i} \quad (1)$$

in which $B_i(T)$ is the radiance of the blackbody at temperature T, $T_i$ is the brightness temperature for channel i, $\varepsilon_i$ and $T_s$ are surface emissivity in channel i and the surface temperature, respectively, $\tau_i$ is the transmittance in channel i, and $R^{\uparrow}_{atm\_i}$ and $R^{\downarrow}_{atm\_i}$ are the upwelling and downwelling atmospheric thermal radiance in channel i, respectively. To obtain ST from (1), the atmospheric effect and LSE must be known or removed in advance. According to the SW algorithm, the atmospheric effect can be removed based on the differential water vapor absorption in the two adjacent TIR channels.

### B. SST RETRIEVAL ALGORITHM

The linear SW algorithm for SST retrieval was first proposed by McMillin in the 1970s. To improve the accuracy of SST retrieval, a nonlinear SW algorithm was developed from satellite TIR data as [28]

$$SST = a_0 + a_1 T_i^2 + a_2 T_j^2 + a_3 T_i \cdot T_j + a_4 T_i + a_5 T_j \quad (2)$$

where SST is the sea surface temperature, $T_i$ and $T_j$ are the TOA brightness temperatures in TIR channels i and j, respectively, and $a_0 \sim a_5$ are fitting coefficients.

### C. LST RETRIEVAL ALGORITHM

Wan *et al.* first used a GSW algorithm to retrieve LST based on the differential water vapor absorption in two adjacent TIR channels. Then they refined this method by adding a quadratic term of the difference between two TIR brightness temperatures to improve the accuracy. Therefore, in this study, the widely used GSW algorithm is selected, this algorithm can be written as [37]

$$\begin{aligned} T_s = {} & b_0 + (b_1 + b_2 \frac{1-\varepsilon}{\varepsilon} + b_3 \frac{\Delta\varepsilon}{\varepsilon^2})(\frac{T_i + T_j}{2}) \\ & + (b_4 + b_5 \frac{1-\varepsilon}{\varepsilon} + b_6 \frac{\Delta\varepsilon}{\varepsilon^2})(\frac{T_i - T_j}{2}) + b_7 (T_i - T_j)^2 \end{aligned} \quad (3)$$

with $\varepsilon = (\varepsilon_i + \varepsilon_j)/2$, $\Delta\varepsilon = \varepsilon_i - \varepsilon_j$.
where $\varepsilon_i$ and $\varepsilon_j$ are the LSEs in channels i and j, respectively, $\varepsilon$ is the averaged emissivity, $\Delta\varepsilon$ is the emissivity difference between the two TIR channels, and $b_i$(i = 0∼7) is the unknown coefficient that can be derived from simulated data.

### D. LSE ESTIMATION

LSE is a crucial factor in the retrieval of LST. It can be seen from (1) that LSE must be corrected before LST retrieval. However, LST and LSE are coupled together through the RTE, and it is quite difficult to separate the two parameters. Tang *et al.* used an improved normalized difference vegetation index (NDVI)-based threshold method to retrieve LSE [38]. In this method, the pixels are divided into three kinds: bare soil pixels, dense vegetation pixels, and soil/vegetation mixed pixels. For the bare soil pixels, LSE is estimated from the relationship between the visible/near-infrared channel reflectances and TIR emissivities (see (4)). For the dense vegetation pixels, LSE is calculated by the relationship between the TIR emissivities and NDVI for dense vegetation ($NDVI_v$) (see (5)). For the soil/vegetation mixed

pixels, LSE is calculated according to the proportion of bare soil to vegetation (see (6)). LSE can be calculated as:

$$\varepsilon_{si} = a_{i0} + \sum_{j=1}^{n} a_{ij}\rho_j \tag{4}$$

$$\varepsilon_{vi} = b_{i0} + NDVI_v \tag{5}$$

$$\varepsilon_i = \varepsilon_{vi}P_v + \varepsilon_{si}(1 - P_v) + C_i \tag{6}$$

where $\varepsilon_{si}$ represents emissivity of bare soil in the pixel for TIR channel i, $a_{i0}$ and $a_{ij}$ are the regression coefficients for TIR channel i, $\rho_j$ is visible/near-infrared reflectance in channel j, and n means that there are $n$ visible/near-infrared channels. The value $\varepsilon_{vi}$ represents the emissivity of dense vegetation in the pixel for TIR channel i, $b_{i0}$ is the regression coefficient for TIR channel i, and $\varepsilon_i$ is the emissivity of the soil/vegetation mixed pixel for TIR channel i.

$P_v$ is the vegetation proportion, and it can be calculated from:

$$P_v = [\frac{NDVI - NDVI_s}{NDVI_v - NDVI_s}]^2 \tag{7}$$

where $NDVI_v$ and $NDVI_s$ are the values for full vegetation and bare soil pixels, respectively. In this part, $NDVI_v$ and $NDVI_s$ are set to be 0.86 and 0.2, respectively. This means that if the NDVI value is less than 0.2, the pixel is regarded as a bare soil pixel, while the full vegetation pixel is determined with an NDVI larger than 0.86. NDVI can be calculated from the red and near-infrared reflectance.

The term $C_i$ in (6) includes the effect of geometrical distribution on natural surfaces and internal reflections, expressed as

$$C_i = (1 - \varepsilon_{si})(1 - P_v)F\varepsilon_{vi} \tag{8}$$

where $F$ is a shape factor ranging from 0 to 1, and normally to be set as a mean value of 0.55.

### *E. DATA SIMULATION*

The MODTRAN 5.0 radiative transfer code is used to predict the brightness temperatures at TOA to obtain the coefficients in (2) and (3). A set of 545 radiosounding profiles (only clear-sky conditions with atmospheric bottom temperatures ($T_a$) ranging from 260 K to 310 K and water vapor content (WVC) ranging from 0.06 g/cm$^2$ to 5.39g/cm$^2$ are taken into consideration) are extracted from the TOVS Initial Guess Retrieval (TIGR) database to analyze atmospheric effects. To make the simulation data closer to the real situations, the LSTs are made with the rule that the LSTs range from $T_a - 5K$ to $T_a + 15K$ with a step of 5 K, whereas the SSTs range from $T_a - 4K$ to $T_a + 4K$ with a step of 2 K. Furthermore, 70 different emissivities (soils, vegetation, water, etc.) obtained from the Johns Hopkins University (JHU) Spectral library are considered. To determine the coefficients, WVC is divided into five sub-ranges, namely, [0-1.5], [1-2.5], [2-3.5], [3-4.5], and [4-5.5] g/cm$^2$, to improve the fitting accuracy. Considering that the GF5 satellite observes the earth almost at nadir, the view zenith angle (VZA) is set to be 0° in MODTRAN 5.0.

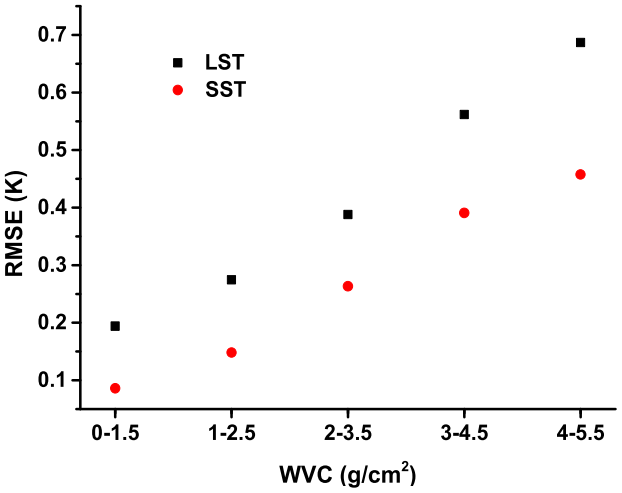


**FIGURE 1.** RMSEs of SST and LST retrieval.

**TABLE 1.** SST retrieval algorithm Coefficients in (2) in different WVC subranges.

| WVC (g/cm$^2$) | 0-1.5 | 1-2.5 | 2-3.5 | 3-4.5 | 4-5.5 |
|---|---|---|---|---|---|
| $a_0$ | -12.97 | 13.89 | -38.29 | 226.87 | 275.72 |
| $a_1$ | -0.24 | 0.18 | -0.07 | -0.04 | 0.05 |
| $a_2$ | -0.25 | 0.20 | -0.07 | 0.00 | 0.09 |
| $a_3$ | 0.49 | -0.38 | 0.13 | 0.05 | -0.14 |
| $a_4$ | -0.47 | 9.50 | 3.83 | 16.31 | 14.98 |
| $a_5$ | 1.56 | -8.61 | -2.55 | -16.88 | -15.95 |

**TABLE 2.** LST retrieval algorithm Coefficients in (3) in different WVC subranges.

| WVC (g/cm$^2$) | 0-1.5 | 1-2.5 | 2-3.5 | 3-4.5 | 4-5.5 |
|---|---|---|---|---|---|
| $b_0$ | -3.59 | -1.14 | 8.37 | 3.79 | -14.56 |
| $b_1$ | 1.02 | 1.00 | 0.97 | 0.98 | 1.05 |
| $b_2$ | 0.15 | 0.15 | 0.14 | 0.10 | 0.08 |
| $b_3$ | -0.43 | -0.41 | -0.33 | -0.18 | -0.11 |
| $b_4$ | 4.58 | 5.78 | 7.34 | 7.97 | 7.62 |
| $b_5$ | 10.89 | 7.61 | 6.26 | 8.70 | 8.11 |
| $b_6$ | 16.50 | 6.94 | -7.05 | -20.97 | -18.44 |
| $b_7$ | -0.10 | -0.07 | -0.06 | -0.07 | 0.04 |

Fig. 1 shows the RMSEs of SST and LST retrieval using the coefficients of (2) and (3) obtained from simulation data (see Table 1 and Table 2). The accuracies of SST retrieval are better than those of LST retrieval in all WVC subranges. The RMSEs increase with increasing WVC for both SST and LST retrieval. The minimum RMSE for SST (LST) retrieval is 0.09 K (0.19 K) and appears in the subrange of WVC $\in$ [0-1.5 g/cm$^2$], while the maximum RMSE for SST (LST) retrieval is 0.46 K (0.69 K) appears in the subrange of WVC $\in$ [4-5.5 g/cm$^2$].

### F. SENSITIVITY ANALYSIS

The LST and SST retrieval accuracies are mainly affected by the instrument noise equivalent difference temperature (NE$\Delta$T), and the uncertainties of LSEs and WVCs. In this section, the uncertainties of NE$\Delta$T, LSE, and WVC for ST retrieval are investigated.

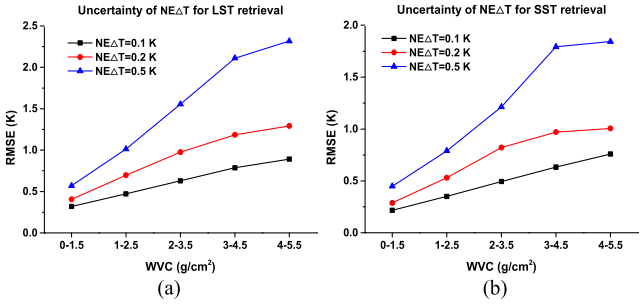


**FIGURE 2.** ST retrieval error caused by NE$\Delta$T for: (a) LST retrieval. (b) SST retrieval.

Fig. 2 shows the impact of NE$\Delta$T on ST retrieval. The RMSEs increase for both SST and LST retrieval as NE$\Delta$T increases. The NE$\Delta$T of 0.1 K, 0.2 K, and 0.5 K can produce the errors ranging from 0.32 K to 0.89 K (0.21 K to 0.76 K), 0.41 K to 1.29 K (0.29 K to 1.00 K), and 0.57 K to 2.32 K (0.45 K to 1.84 K) for LST (SST) retrieval, respectively.

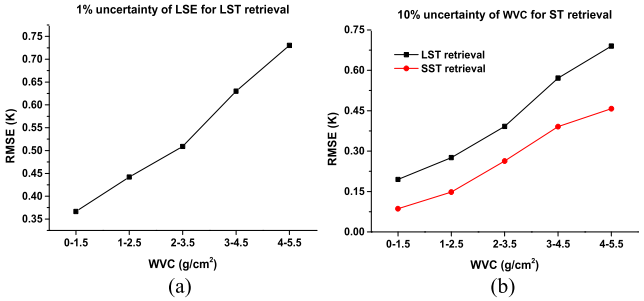


**FIGURE 3.** ST retrieval error caused by LSE and WVC. (a) LST retrieval error caused by LSE. (b) LST and SST retrieval errors caused by WVC.

The errors caused by the uncertainties of LSE and WVC are shown in Fig. 3. The results demonstrate that an uncertainty of 1% in the LSEs causes an error ranges from 0.37 K to 0.73 K for LST retrieval; an uncertainty of 10% in the WVCs can produce errors ranging from 0.19 K to 0.69 K (0.09 K to 0.46 K) for LST (SST) retrieval, respectively. Both errors increase with increasing WVCs.

Considering the instrument noises ($\delta(LST_{NE\Delta T})$), the uncertainties of LSEs ($\delta(LST_{\varepsilon})$) and WVCs ($\delta(LST_{WVC})$), and the accuracy of the algorithm ($\delta(LST_r)$), the overall error on the ST ($\delta(ST)$) can be described as follows:

$$\delta(ST) = \sqrt{\delta^2(LST_r) + \delta^2(LST_{NE\Delta T}) + \delta^2(LST_{\varepsilon}) + \delta^2(LST_{WVC})} \quad (9)$$

Fig. 4 shows the overall errors in LST and SST retrieval. It can be seen from Fig. 4(a) that the maximum RMSE is approximately 2.5 K for the uncertainties of NE$\Delta$T: 0.5 K, LSE: 1%, and WVC: 10%; the minimum RMSE is approximately 0.46 K for the uncertainties of NE$\Delta$T: 0.1 K, LSE: 1%, and WVC: 10%. Fig. 4(b) shows the overall errors in SST retrieval without LSE error. The figure demonstrates that the maximum RMSE is approximately 1.9 K for the uncertainties of NE$\Delta$T: 0.5 K and WVC: 10%; the minimum RMSE is approximately 0.21 K for the uncertainties of NE$\Delta$T: 0.1 K and WVC: 10%. Because the uncertainty of WVC has relatively little influence on SST retrieval, the overall error is mostly caused by NE$\Delta$T.

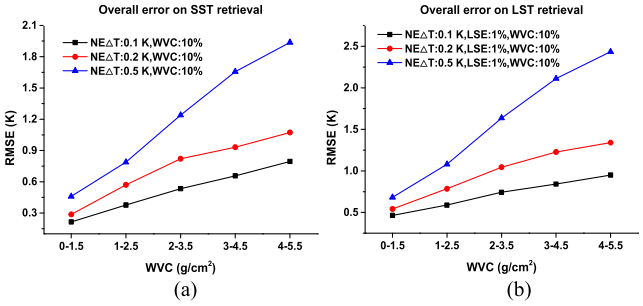


**FIGURE 4.** Overall errors on ST retrieval for: (a) LST retrieval. (b) SST retrieval.

## III. PRELIMINARY APPLICATION TO GF5 DATA

### A. CROSS-CALIBRATION

To obtain the LST and SST information, radiometric calibration is the first and most important step. Because of the unserviceable official calibration coefficients for GF5 images, the VIIRS TIR images are used for cross-calibration because of the high calibration accuracy. Fig. 5 displays the spectralresponse functions of VIIRS TIR (bands 15 and 16) and GF5 TIR (bands 9, 10, 11, and 12). GF5 bands 11 and 12 are selected as the ST retrieval bands due to the similarity between GF5 bands 11 and 12 and VIIRS bands 15 and 16.

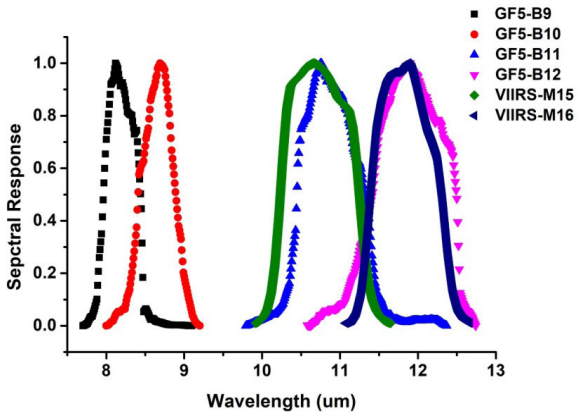


**FIGURE 5.** Spectral response functions of VIIRS and GF5.

Because of the difference between the spectral response functions of VIIRS and GF5, 70 different emissivities and atmospheric profiles with WVC $\in$ [0-1.5 g/cm$^2$] are used to calculate the spectral matching factor. Fig. 6 shows the

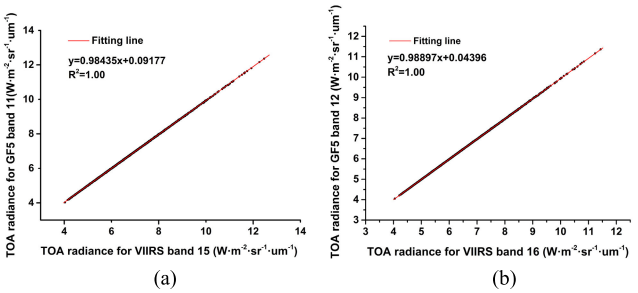


**FIGURE 6.** Spectral matching factors for GF5 TIR bands for: (a) GF5 band 11. (b) GF5 band 12.

spectral matching factors for VIIRS bands 15 and 16. We can see that for VIIRS band 15 (16), the slope is 0.98435 (0.98897) and the intercept is 0.09177 (0.04396). Therefore, the GF5 TIR radiances can be obtained using the two empirical relationships below from VIIRS TIR images.

$$R_{11}^{G} = 0.98435 \cdot R_{15}^{V} + 0.09177 \tag{10}$$

$$R_{12}^{G} = 0.98897 \cdot R_{16}^{V} + 0.04396 \tag{11}$$

where $R_{11}^{G}$ and $R_{12}^{G}$ are the radiances of GF5 TIR data and $R_{15}^{V}$ and $R_{16}^{V}$ are the radiances of VIIRS TIR data.

For GF5 TIR channel i, the relationship between the TOA radiance and the image digital number (DN) can be written as:

$$R_{i}^{G} = Gain \cdot DN_{j} + Offset \tag{12}$$

where $DN_j$ is the DN value in pixel j and the value of *Offset* is assumed to be 0 in this article, $R_i^G$ is the TIR radiance in channel i of GF5.

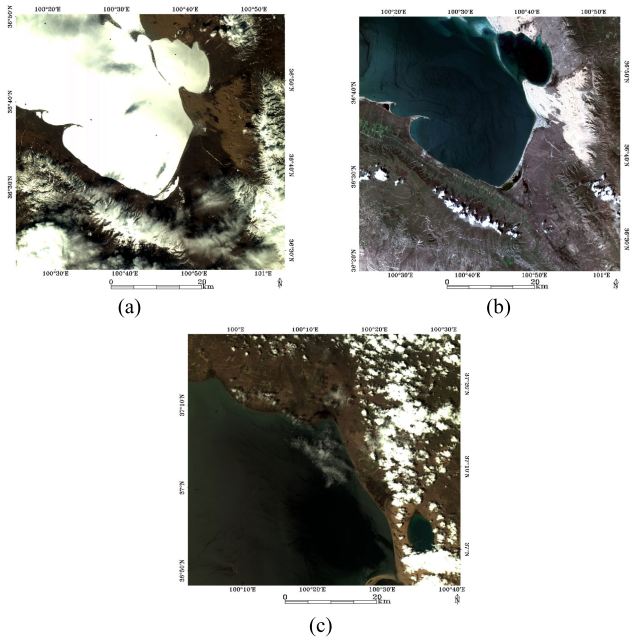


**FIGURE 7.** False-color images for GF5 (sites for SST retrieval). Imaging time: (a) for 20190308. (b) for 20190625. (c) for 20190815.

To derive the cross-calibration coefficient *Gain*, a common calibration area is selected. In this article, only 7 clear-sky

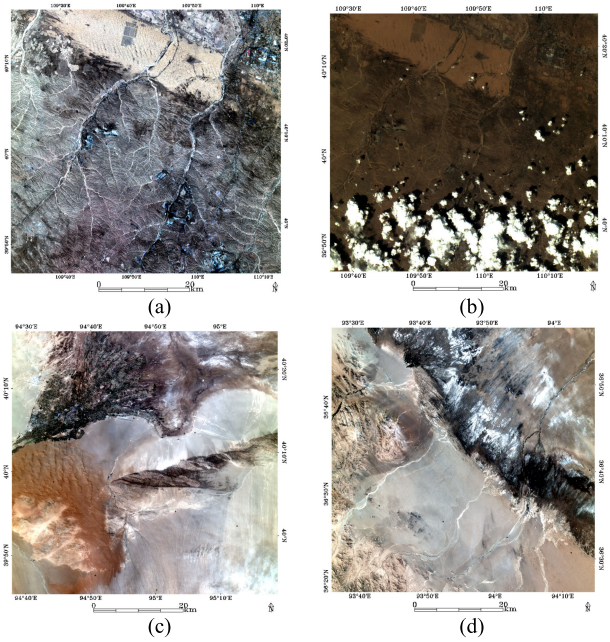


**FIGURE 8.** False-color images for GF5 (sites for LST retrieval). Imaging time: (a) for 20190314. (b) for 20190504. (c) for 20190517. (d) for 20190811.

**TABLE 3.** Calibration coefficients (Gain).

| | Imaging time | Gain for GF5 band 11 | Gain for GF5 band 12 |
|---|---|---|---|
| Images for SST retrieval | 20190308 | 0.001557692 | 0.0018254 |
| | 20190625 | 0.002587222 | 0.002694646 |
| | 20190815 | 0.002649991 | 0.002763602 |
| Images for LST retrieval | 20190314 | 0.002266186 | 0.002632684 |
| | 20190504 | 0.002959378 | 0.00327855 |
| | 20190517 | 0.003418199 | 0.003938613 |
| | 20190811 | 0.004097023 | 0.004299967 |

GF5 TIR images are available for retrieving STs: three images of the Qinghai Lake (see Fig. 7) for SST retrieval, and four images of Dalat, Dunhung, and Geermu (see Fig. 8) for LST retrieval. First, the spatial resolution of GF5 and VIIRS TIR images should be matched. Then calibration sites including 6 × 6 pixels covered by soil (for LST retrieval) and sea water (for SST retrieval) are selected to calculate the coefficients. Based on the mean value of DNs for GF5 and radiances obtained from VIIRS radiances using (10) and (11) in the calibration sites, the calibration coefficient (*Gain*) can be derived from (12). From the results, it can be found that the calibration coefficients are not the same for different days (see Table 3); therefore, radiometric calibration should be carried out for each GF5 image.

### B. RESULTS AND VALIDATION

After data processing, the SSTs and LSTs can be derived using (2) and (3) from the real GF5 TIR data, respectively. The coefficients of the two retrieval algorithms are both determined by the WVC. In this part, the MODIS WVC product is used to obtain information on the water vapor content.

The MODIS level-2 atmospheric precipitable water product consists of total atmospheric column water vapor amounts over clear land and oceanic areas of the globe, and the short name for this level-2 MODIS total precipitable water vapor product is MYD05 [39]. Based on MYD05, the coefficients can be selected.

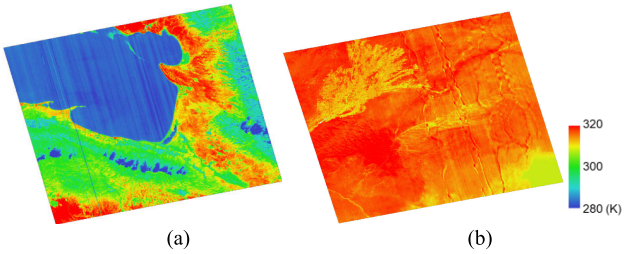


**FIGURE 9.** ST retrieval for the real GF5 observations for (a) SST retrieval, imaging time: 20190815. (b) LST retrieval, imaging time: 20190517.

Fig. 9 shows the SST and LST retrieval results for different underlying surfaces. It is obvious that for the same day, the temperature of water is lower than that of soil and rock. The temperature of the soil is higher than that of vegetation. A possible reason is the specific heat capacity of water is higher than those of vegetation and soil. Water can absorb or release a large quantity of heat energy with little change in temperature. Thus, under the same radiation conditions, the temperature of the water body is lower than the other two kinds of underlying surface temperatures.

Because of the lack of *in situ* measurements, MODIS LST products (short name: MYD11A1) are used to cross-validate the STs retrieved from GF5 TIR data. The MYD11A1 Version 6 product provides daily per-pixel land surface temperature and emissivity (LST&E) with 1 kilometer (km) spatial resolution in a 1,200 by 1,200 km grid [37], [40]. The MODIS reprojection tool (MRT) was used to transform the sinusoidal projection (which is used in the LST products) onto a geographic projection (which is used in the GF5 images). For the MYD11A1 product, the scientific data sets of the daytime LSTs and quality control (QC) are selected.

Due to the spatial resolution difference between the retrieved STs and MODIS LST products, equation (13) is used to make them to the same resolution.

$$ST = \sum_{j=1}^{N} \omega_j ST_j \Big/ \sum_{j=1}^{N} \omega_j \quad with \quad \omega_j = S_{j,p}/S_j \tag{13}$$

where $ST$ is the aggregated target pixel value, N is the total pixel number in the target pixel, $\omega_j$ is the weight of pixel j, $S_{j,p}$ is the partial area of pixel j overlapping with the target pixel, $S_j$ is the total area of pixel j, and $ST_j$ is the temperature information of the pixel j.

Additionally, the QC value of MODIS LST product is used to decide whether the aggregated retrieved ST is selected. The aggregated pixel is recognized as useful when QC equals 0 in this study.

Fig. 10 and 11 show the RMSEs of MODIS STs minus retrieved STs. From Fig. 10, it can be found that the RMSE for

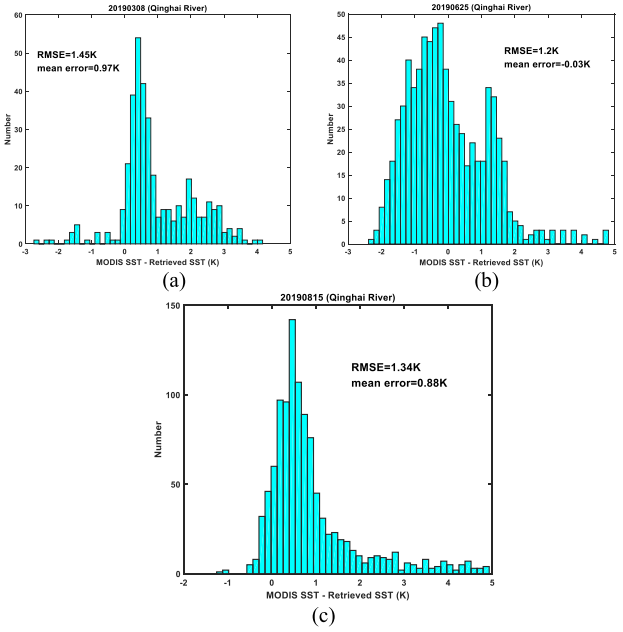


**FIGURE 10.** Results of cross-validation for SST retrieval (Qinghai Lake). Imaging time: (a) 20190308. (b) 20190625. (c) 20190815.

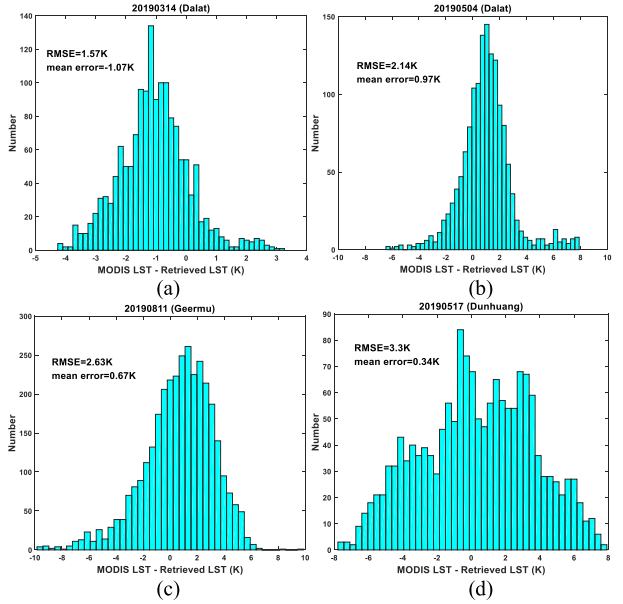


**FIGURE 11.** Results of cross-validation for LST retrieval. Imaging time: (a) 20190314, Dalat. (b) 20190504, Dalat. (c) 20190517, Dunhuang. (d) 20190811, Geermu.

SST retrieval ranges from 1.2 K to 1.45 K with a mean value of 1.33 K. The figures in Fig. 11 demonstrate that the RMSE for LST retrieval ranges from 1.57 K to 3.3 K with a mean value of 2.41 K. We can see that there are some differences between MODIS STs and the retrieved STs, which may be due to the following: 1) the difference on imaging times of MODIS and GF5 is approximately 30 minutes, which can lead to different radiation for the two TIR images; or 2) there is a large difference in spatial resolution for the two datasets, which may produce some errors during the process of upscaling. Furthermore, it is obvious that the accuracy

of SST retrieval is better than that of LST retrieval. The possible reason for this result is that water emissivity is higher than the emissivity of soil and rock, and the SST can also be retrieved by assuming the water emissivity as a constant value, while the LSE must be known in advance for LST retrieval. Therefore, the effect of emissivity uncertainty for SST retrieval is less than that for LST retrieval.

## IV. CONCLUSION

In this study, the nonlinear SW algorithm and the refined GSW method are used to retrieve SST and LST, respectively, for real GF5 TIR images. The coefficients of the two algorithms are calculated using a statistical regression method from the numerical values simulated with the atmospheric radiative transfer model MODTRAN 5.0 under different atmospheric and surface conditions. From the simulation results, it can be seen that the RMSEs for SST (LST) retrieval range from 0.09 K(0.19 K) to 0.46 K (0.69 K) as the WVC increases. In addition, the sensitivity analysis is performed in terms of NE$\Delta$T, the uncertainty of the LSE and WVC. The results show that when WVC ranges from 0 g/cm$^2$ to 1.5 g/cm$^2$, an NE$\Delta$T of 0.1 K, 0.2 K, and 0.5 K can produce 0.32 K (0.21 K), 0.41 K (0.29 K), and 0.57 K (0.48 K) for LST (SST) retrieval; an uncertainty of 10% in the WVCs will result in an error of 0.20 K and 0.09 K for LST retrieval and SST retrieval, respectively; an uncertainty of 1% in the LSEs carries an error ranging from 0.37 K to 0.73 K for LST retrieval.

Finally, the two algorithms are applied to the real GF5 TIR images covered by water and soil. Due to the unserviceable official calibration coefficients for GF5 TIR images, GF5 images are cross-calibrated by VIIRS TIR images. Additionally, the TIR LSE is obtained with the help of GF5 visible images. Unfortunately, *in situ* measurements are unavailable, and the MODIS LST product MYD11A1 is used for cross-validation. From the cross-validation results, it can be seen that both RMSEs of LST and SST are less than 3.3 K, which are caused by the difference on imaging times of MODIS and GF5, and the difference in spatial resolution for the two datasets. The RMSE for SST retrieval varies from 1.2 K to 1.45 K with a mean value of 1.33 K, and the RMSE for LST retrieval is from 1.57 K to 3.3 K with a mean value of 2.41 K. The results indicate that the two ST retrieval methods can be applied to real GF5 TIR observations, and the retrieval accuracy is less than 3.3 K. Notably, the calibration coefficients are unstable for the TIR images of different days; therefore, the radiometric calibration should be carried out for each GF5 image.

In the future, more GF5/MSI images would be used for LST retrieval using the Temperature Emissivity Separation (TES) algorithm, and the corresponding in situ measurements will be collected for validating the retrieved LST. Meanwhile, these factors related to RMSE for LST retrieval in each site would be quantitatively analyzed.

## REFERENCES

[1] W. Li, L. Ni, Z.-L. Li, S.-B. Duan, and H. Wu, "Evaluation of machine learning algorithms in spatial downscaling of MODIS Land Surface Temperature," *IEEE J. Sel. Topics Appl. Earth Observ. Remote Sens.*, vol. 12, no. 7, pp. 2299–2307, Jul. 2019.

[2] M. Lemus-Canovas, J. Martin-Vide, M. C. Moreno-Garcia, and J. A. Lopez-Bustins, "Estimating Barcelona's metropolitan daytime hot and cold poles using Landsat-8 Land surface temperature," *Sci. Total Environ.*, vol. 699, Jan. 2020, Art. no. 134307.

[3] Y. Zhang and L. Sun, "Spatial-temporal impacts of urban land use land cover on Land Surface Temperature: Case studies of two canadian urban areas," *Int. J. Appl. Earth Observ. Geoinformation*, vol. 75, pp. 171–181, Mar. 2019.

[4] W. Zhao, S.-B. Duan, A. Li, and G. Yin, "A practical method for reducing terrain effect on Land Surface Temperature using random forest regression," *Remote Sens. Environ.*, vol. 221, pp. 635–649, Feb. 2019.

[5] A. Sekertekin and S. Bonafoni, "Land Surface Temperature retrieval from landsat 5, 7, and 8 over rural areas: Assessment of different retrieval algorithms and emissivity models and toolbox implementation," *Remote Sens.*, vol. 12, no. 2, p. 294, Jan. 2020.

[6] S.-B. Duan, Z.-L. Li, H. Li, F.-M. Göttsche, H. Wu, W. Zhao, P. Leng, X. Zhang, and C. Coll, "Validation of collection 6 MODIS Land Surface Temperature product using *in situ* measurements," *Remote Sens. Environ.*, vol. 225, pp. 16–29, May 2019.

[7] E. Zhao, C. Gao, X. Jiang, and Z. Liu, "Land Surface Temperature retrieval from AMSR-E passive microwave data," *Opt. Exp.*, vol. 25, no. 20, p. A940, Oct. 2017.

[8] F.-C. Zhou, Z.-L. Li, H. Wu, S.-B. Duan, X. Song, and G. Yan, "A practical two-stage algorithm for retrieving land surface temperature from AMSR-E Data—A case study over China," *IEEE J. Sel. Topics Appl. Earth Observ. Remote Sens.*, vol. 11, no. 6, pp. 1939–1948, Jun. 2018.

[9] M. R. Saradjian and Y. Jouybari-Moghaddam, "Land Surface Emissivity and temperature retrieval from Landsat-8 satellite data using Support Vector Regression and weighted least squares approach," *Remote Sens. Lett.*, vol. 10, no. 5, pp. 439–448, Feb. 2019.

[10] M. Anderson, J. Norman, W. Kustas, R. Houborg, P. Starks, and N. Agam, "A thermal-based remote sensing technique for routine mapping of land-surface carbon, water and energy fluxes from field to regional scales," *Remote Sens. Environ.*, vol. 112, no. 12, pp. 4227–4241, Dec. 2008.

[11] J. Cheng, S. Liang, J. Wang, and X. Li, "A stepwise refining algorithm of temperature and emissivity separation for hyperspectral thermal infrared data," *IEEE Trans. Geosci. Remote Sens.*, vol. 48, no. 3, pp. 1588–1597, Mar. 2010.

[12] S.-B. Duan, Z.-L. Li, C. Wang, S. Zhang, B.-H. Tang, P. Leng, and M.-F. Gao, "Land-surface temperature retrieval from landsat 8 single-channel thermal infrared data in combination with NCEP reanalysis data and ASTER GED product," *Int. J. Remote Sens.*, vol. 40, nos. 5–6, pp. 1763–1778, Mar. 2019.

[13] P. Sismanidis, B. Bechtel, I. Keramitsoglou, and C. T. Kiranoudis, "Mapping the spatiotemporal dynamics of Europe's land surface temperatures," *IEEE Geosci. Remote Sens. Lett.*, vol. 15, no. 2, pp. 202–206, Feb. 2018.

[14] C. Huang, S.-B. Duan, X.-G. Jiang, X.-J. Han, H. Wu, M. Gao, P. Leng, and Z.-L. Li, "Intercomparison of AMSR2- and MODIS-derived Land Surface Temperature under clear-sky conditions," *IEEE J. Sel. Topics Appl. Earth Observ. Remote Sens.*, vol. 12, no. 9, pp. 3286–3294, Sep. 2019.

[15] D. Stroppiana, M. Antoninetti, and P. A. Brivio, "Seasonality of MODIS LST over southern Italy and correlation with land cover, topography and solar radiation," *Eur. J. Remote Sens.*, vol. 47, no. 1, pp. 133–152, Jan. 2014.

[16] X. Zhang, C. Wang, H. Zhao, and Z. H. Lu, "Retrievals of all-weather daytime land surface temperature from FengYun-2D data," *Opt. Exp.*, vol. 25, no. 22, pp. 27210–27224, Oct. 2017.

[17] M. Neteler, "Estimating daily land surface temperatures in mountainous environments by reconstructed MODIS LST data," *Remote Sens.*, vol. 2, no. 1, pp. 333–351, Jan. 2010.

[18] S.-B. Duan, Z.-L. Li, B.-H. Tang, H. Wu, and R. Tang, "Generation of a time-consistent Land Surface Temperature product from MODIS data," *Remote Sens. Environ.*, vol. 140, pp. 339–349, Jan. 2014.

[19] Y. Qian, N. Wang, K. Li, H. Wu, S. Duan, Y. Liu, L. Ma, C. Gao, S. Qiu, L. Tang, and C. Li, "Retrieval of surface temperature and emissivity from ground-based time-series thermal infrared data," *IEEE J. Sel. Topics Appl. Earth Observ. Remote Sens.*, vol. 13, no. 4, pp. 284–292, Jan. 2020.

[20] E. Zhao, Y. Qian, C. Gao, H. Huo, X. Jiang, and X. Kong, "Land Surface Temperature retrieval using airborne hyperspectral scanner daytime mid-infrared data," *Remote Sens.*, vol. 6, no. 12, pp. 12667–12685, Dec. 2014.
[21] W. G. M. Bastiaanssen, M. Menenti, R. A. Feddes, and A. A. M. Holtslag, "A remote sensing surface energy balance algorithm for land (SEBAL). 1. formulation," *J. Hydrol.*, vols. 212–213, pp. 198–212, Dec. 1998.
[22] G. C. Hulley, N. K. Malakar, T. Islam, and R. J. Freepartner, "NASA's MODIS and VIIRS Land surface temperature and emissivity products: A long-term and consistent Earth system data record," *IEEE J. Sel. Topics Appl. Earth Observ. Remote Sens.*, vol. 11, no. 2, pp. 522–535, Feb. 2018.
[23] S.-B. Duan, Z.-L. Li, and P. Leng, "A framework for the retrieval of all-weather land surface temperature at a high spatial resolution from polar-orbiting thermal infrared and passive microwave data," *Remote Sens. Environ.*, vol. 195, pp. 107–117, Jun. 2017.
[24] L. M. Mcmillin, "Estimation of sea surface temperatures from two infrared window measurements with different absorption," *J. Geophys. Res.*, vol. 80, no. 36, pp. 5113–5117, Dec. 1975.
[25] Z. Wan and J. Dozier, "A generalized split-window algorithm for retrieving land-surface temperature from space," *IEEE Trans. Geosci. Remote Sens.*, vol. 34, no. 4, pp. 892–905, Jul. 1996.
[26] X. Meng and J. Cheng, "Estimating land and sea surface temperature from cross-calibrated Chinese Gaofen-5 thermal infrared data using split-window algorithm," *IEEE Geosci. Remote Sens. Lett.*, vol. 17, no. 3, pp. 509–513, Mar. 2020.
[27] Y. Chen, S.-B. Duan, H. Ren, J. Labed, and Z.-L. Li, "Algorithm development for land surface temperature retrieval: Application to Chinese Gaofen-5 data," *Remote Sens.*, vol. 9, no. 2, p. 161, Feb. 2017.
[28] Y. Chen, S.-B. Duan, J. Labed, and Z.-L. Li, "Development of a split-window algorithm for estimating sea surface temperature from the Chinese Gaofen-5 data," *Int. J. Remote Sens.*, vol. 40, nos. 5–6, pp. 1621–1639, Aug. 2018.
[29] S. S. Miao, "Gaofen 5 and Gaofen 6 satellites put into operation," *Aerosp. China*, vol. 20, no. 1, p. 58, Feb. 2019.
[30] C. Zhang, C. Liu, Y. Wang, F. Si, H. Zhou, M. Zhao, W. Su, W. Zhang, K. L. Chan, X. Liu, P. Xie, J. Liu, and T. Wagner, "Preflight evaluation of the performance of the Chinese environmental trace gas monitoring instrument (EMI) by spectral analyses of nitrogen dioxide," *IEEE Trans. Geosci. Remote Sens.*, vol. 56, no. 6, pp. 3323–3332, Jun. 2018.
[31] X. F. Yang. (Jun. 2019). *Air Quality Impact Assessment of Mining Area using Gaofen-5 Satellite*. [Online]. Available: https://kns.cnki.net/KCMS/detail/detail.aspx?dbcode=IPFD&filename=DXHD201906001264
[32] E. Y. Zhao, C. X. Gao, and Y. Y. Yao, "New land surface temperature retrieval algorithm for heavy aerosol loading during nighttime from Gaofen-5 satellite data," *Opt. Exp.*, vol. 28, no. 2, pp. 2583–2599, Jan. 2020.
[33] B.-H. Tang, "Nonlinear split-window algorithms for estimating land and sea surface temperatures from simulated Chinese Gaofen-5 satellite data," *IEEE Trans. Geosci. Remote Sens.*, vol. 56, no. 11, pp. 6280–6289, Nov. 2018.
[34] X. Ye, H. Ren, R. Liu, Q. Qin, Y. Liu, and J. Dong, "Land Surface Temperature estimate from Chinese Gaofen-5 satellite data using split-window algorithm," *IEEE Trans. Geosci. Remote Sens.*, vol. 55, no. 10, pp. 5877–5888, Oct. 2017.
[35] H. Ren, X. Ye, R. Liu, J. Dong, and Q. Qin, "Improving Land Surface Temperature and emissivity retrieval from the Chinese Gaofen-5 satellite using a hybrid algorithm," *IEEE Trans. Geosci. Remote Sens.*, vol. 56, no. 2, pp. 1080–1090, Feb. 2018.
[36] Z.-L. Li, B.-H. Tang, H. Wu, H. Ren, G. Yan, Z. Wan, I. F. Trigo, and J. A. Sobrino, "Satellite-derived land surface temperature: Current status and perspectives," *Remote Sens. Environ.*, vol. 131, pp. 14–37, Apr. 2013.
[37] Z. Wan, "New refinements and validation of the collection-6 MODIS land-surface temperature/emissivity product," *Remote Sens. Environ.*, vol. 140, pp. 36–45, Jan. 2014.
[38] B. H. Tang, K. Shao, Z. L. Li, H. Wu, and R. Tang, "An improved NDVI-based threshold method for estimating land surface emissivity using MODIS satellite data," *Int. J. Remote Sens.*, vol. 36, nos. 19–20, pp. 1–15, Oct. 2015.
[39] S.-H. Chen, Z. Zhao, J. S. Haase, A. Chen, and F. Vandenberghe, "A study of the characteristics and assimilation of retrieved MODIS total precipitable water data in severe weather simulations," *Monthly Weather Rev.*, vol. 136, no. 9, pp. 3608–3628, Sep. 2008.
[40] H. Li, R. Li, Y. Yang, B. Cao, Z. Bian, T. Hu, Y. Du, L. Sun, and Q. Liu, "Temperature-based and radiance-based validation of the collection 6 MYD11 and MYD21 Land Surface Temperature products over barren surfaces in northwestern China," *IEEE Trans. Geosci. Remote Sens.*, early access, Jun. 12, 2020, doi: 10.1109/TGRS.2020.2998945.

**ENYU ZHAO** received the Ph.D. degree from the College of Resources and Environment, University of Chinese Academy of Sciences, Beijing, China, in 2017, and the joint Ph.D. degree in cartography and geographic information system from the University of Chinese Academy of Sciences, and from the Engineering Science, Computer Science and Imaging Laboratory, University of Strasbourg, Strasbourg, France.

He is currently a Lecturer with the College of Information Science and Technology, Dalian Maritime University, Dalian, China. His research interests include quantitative remote sensing and hyperspectral image processing.

**QIJIN HAN** received the B.S. degree in mechanical and electronics engineering from Chang'an University, Xi'an, China, in 2007, and the M.S. degree in aircraft design from the China Academy of Space Technology, Beijing, China, in 2010.He is currently an Associate Professor with the China Center for Resources Satellite Data and Application, Beijing. His research interests include radiometric calibration and validation of remote sensors, data processing, and quantitative applications of remotely sensed images.

**CAIXIA GAO** received the B.S. degree in electronic and information engineering from the Xi'an University of Posts and Telecommunications, Xi'an, China, in 2006, the M.S. degree in computer science from the Academy of Opto-Electronics, Chinese Academy of Sciences, Beijing, China, in 2009, and the Ph.D. degree in cartography and geography information system from the University of Chinese Academy of Sciences, Beijing, in 2012.

She is currently an Associate Professor with the Aerospace Information Research Institute, Chinese Academy of Sciences. Her research interests include in-orbit calibration and validation of optical sensors and the retrieval of surface temperature and emissivity.